Riemannian Framework for Estimating Symmetric Positive Definite 4th Order Diffusion Tensors

Aurobrata Ghosh[1], Maxime Descoteaux[2], and Rachid Deriche[1]

[1] Odyssee, INRIA Sophia Antipolis, France
Aurobrata.Ghosh@sophia.inria.fr
[2] NMR Lab, Neurospin, CEA Saclay, France

Abstract. DTI is an important tool to investigate the brain *in vivo* and non-invasively in spite of its shortcomings in regions of fiber-crossings. HARDI models such as QBI and Higher Order Tensors (HOT) were invented to overcome this shortcoming. HOTs, however, have not been explored extensively even though sophisticated estimation schemes were developed for DTI that guarantee positive diffusivity, such as the Riemannian framework. Positive diffusivity is an important constraint in diffusion MRI since it represents the physical phenomenon of molecular diffusion. It seems apt, to leverage the work done on DTI, to apply the positivity constraint to the HOT model. We, therefore, propose to extend the Riemannian framework from DTI to the space of 4th order diffusion tensors. We also review the existing methods for estimating 4th order diffusion tensors and compare all methods on synthetic, phantom and real datasets extensively to test for robustness and speed. Our contributions for extending the Riemannian framework from DTI to estimating 4th order diffusion tensors guarantees positive diffusivity, is robust, is fast, and can be used to discern multiple fiber directions.

1 Introduction

Diffusion Magnetic Resonance Imaging (dMRI) has proved to be an exquisite tool to investigate the anatomical connections of the human nervous system, *in vivo* and non-invasively. Diffusion Tensor Imaging (DTI) [1], was the first model proposed, and its value is only affirmed by its popularity till date. Its limitations are, however, well known in the regions that contain fiber-crossings. Recent High Angular Resolution Diffusion Imaging (HARDI) techniques have overcome that shortcoming with a plethora of new reconstruction schemes such as radial basis functions [2], Spherical Harmonics (SH) [3], Higher Order Tensors (HOT) [4] [5], etc. Notwithstanding its limitations, the DTI model has been extensively explored and sophisticated schemes for estimating it has been developed.

An important constraint in estimating DTI requires it to have a positive diffusivity profile, since it corresponds to the physical phenomenon of diffusion of water molecules. The sophisticated schemes for DTI rely on the native properties of the space of positive definite 2nd order diffusion tensors to guarantee the

D. Metaxas et al. (Eds.): MICCAI 2008, Part I, LNCS 5241, pp. 858–865, 2008.

positive diffusivity profile. It seems appropriate, therefore, to explore HOT while leveraging the extensive framework already established for classical DTI. In this work, we propose a review and a comparison of the existing methods. We also propose an extension of the Riemannian framework [6][7] to the space of 4th order diffusion tensors. We compare our method to the other methods on synthetic, phantom and real data for robustness and speed.

The main contributions are directed towards extending the well established and tested Riemannian framework from DTI-2 to DTI-4. This provides a dMRI estimation method that guarantees positive diffusivity, is robust to noise, is computationally fast, and can also be used to discern multiple fiber directions.

2 Methods

To accommodate a multi-fiber distribution in a voxel, the Gaussian expression of the Stesjkal-Tanner equation was extended in [4], to incorporate a HOT of any order in the diffusivity function, generalizing it to $S = S_0 e^{-bD(\mathbf{g})}$ where $D(\mathbf{g}) = \sum_{j_1=1}^{3}\sum_{j_2=1}^{3}\cdots\sum_{j_k=1}^{3} D_{j_1 j_2 \ldots j_k} g_{j_1} g_{j_2} \ldots g_{j_k} = \mathbf{D}^k$. This generalization of DTI is sometimes referred to as GDTI-2. Another generalization along similar lines was done in [5], where the diffusivity function was written as $D(\mathbf{g}) = \mathbf{D}^2 + i\mathbf{D}^3 + \mathbf{D}^4 + i\mathbf{D}^5 + \ldots$, with $i = \sqrt{-1}$. This approach, sometimes referred to as GDTI-1, however, requires more complex aquisition and reconstruction techniques and therefore, we restrict ourselves to the GDTI-2 model. In GDTI-2 limiting k to 4 results in a 4th order diffusion tensor model. We now review the existing methods for estimating the 4th order diffusion tensor.

2.1 State of the Art

Least Squares (LS). The simplest approach to estimate the coefficients of a HOT, is to solve the over-determined linear least squares inverse problem, as suggested in [4]. This method is fast, is not limited to 4th order diffusion tensors but does not guarantee positive diffusivity, $D(\mathbf{g}) > 0\ \forall \mathbf{g}\ st\ ||\mathbf{g}|| = 1$.

Ternary Quartic (TQ). In [8] the authors are the first to propose a method which guarantees positive diffusivity of the estimated 4th order diffusion tensor. They formulate the diffusivity function as a ternary quartic. Applying Hilbert's theorem on non-negative TQs, the diffusivity function is expressed as $D(\mathbf{g}) = (\mathbf{v}^T\mathbf{q}_1)^2 + (\mathbf{v}^T\mathbf{q}_2)^2 + (\mathbf{v}^T\mathbf{q}_3)^2 = \mathbf{v}^T\mathbf{Q}\mathbf{Q}^T\mathbf{v}$ where $\mathbf{Q}$ is estimated from the HARDI acquisitions, and the coefficients of the 4th order diffusion tensor – $\mathbb{A}$, are extracted from $\mathbf{Q}\mathbf{Q}^T$. Since $\mathbf{Q}$, however, can only determine $\mathbb{A}$ uniquely up to a rotation matrix, it is parameterized as $\mathbf{Q} = [\mathbf{B}, \mathbf{C}]^T = [\mathbf{TR}, \mathbf{C}]^T$ where $\mathbf{TR}$ is the qr-decomposition of $\mathbf{B}$ and $\mathbf{T}$ is taken to be $\mathbf{I}$ to reduce this indeterminacy. However, this method to reduce the number of parameters doesn't seem to have a physical explanation, and other methods may also exist. Also, this approach can only estimate positive semi-definite tensors due to its non-negative TQ formulation.

From Spherical Harmonics (SH). As proposed in [9], it is possible to compute the independent HOT coefficients from the even spherical harmonic coefficients of the same order. Since it is possible to use regularization to estimate the spherical harmonic coefficients, this provides another interesting method for estimating a HOT. This method is also extensible to any order, but again does not assure positive diffusivity.

2.2 Riemannian Approach (RM)

We now propose to extend the Riemannian framework from 2nd order diffusion tensors [6][7] to the space of 4th order tensors. First we consider 4th order tensors to be linear transformations $\mathbb{A} : Lin(V) \rightarrow Lin(V)$, where V is a vector space over $\mathbb{R}^n$ [10]. We can then define the double-dot-product $\mathbb{A} : \mathtt{D} = \mathbb{A}_{ijkl}\mathtt{D}_{kl}$ where $\mathtt{D}$ is a 2nd order tensor (T-2). Then we define the transpose $\langle \mathbb{A} : \mathtt{D} \mid \mathtt{C} \rangle = \langle \mathtt{D} \mid \mathbb{A}^t : \mathtt{C} \rangle$ using the inner-product $\langle . \mid . \rangle$ in the space of T-2s, and also define the inner-product in the space of 4th order tensors $\langle \mathbb{A} \mid \mathbb{B} \rangle = tr(\mathbb{A}^t\mathbb{B})$.

We then study the symmetries of 4th order tensors. As stated in [10] if a 4th order tensor has major and minor symmetries then it has 21 independent coefficients, in three dimensions, and has an eigen decomposition. If it satisfies total symmetry it has 15 independent coefficients. A proposition in [10] states that $\langle \mathbb{A}^s \mid \mathbb{B}^a \rangle = tr(\mathbb{A}^s\mathbb{B}^a) = 0$ where $\mathbb{B}^a$ is the remainder or anti-symmetric part that remains when the totally symmetric part $\mathbb{B}^s$ of a tensor is subtracted from itself $\mathbb{B}$ (see [10]).

When a 4th order tensor $\mathbb{A}$, in three dimensions, satisfies major and minor symmetries it can be mapped to a symmetric T-2 in 6 dimensions [11][10] (6x6) – $\mathtt{A}$. And the double-dot-product $\mathbb{A} : \mathtt{D}$ can be rewritten as a matrix vector product $\mathbb{A} : \mathtt{D} = \mathtt{Ad}$, where $\mathtt{d} = [D_{11}, D_{22}, D_{33}, \sqrt{2}D_{12}, \sqrt{2}D_{13}, \sqrt{2}D_{23}]^T$. We can then rewrite the diffusivity function as $D(\mathbf{g}) = \mathtt{D}_i : \mathbb{A} : \mathtt{D}_i = tr(\mathbb{A}\mathbb{G}_i)$ where $\mathtt{D}_i = g_i \otimes g_i$ with $\otimes$ =outer-product and $\mathbb{G}_i = g_i \otimes g_i \otimes g_i \otimes g_i$ which is totally symmetric. Of course for computations we can use the equivalent matrix formulation $D(\mathbf{g}) = \mathtt{d}_i^t\mathtt{A}\mathtt{d}_i$.

We then proceed exactly as in [6] and estimate $\mathtt{A}$ in $S^+(6)$, the space of symmetric positive definite 6x6 matrices, by using the Riemannian metric defined in that space, with an M-estimator Ψ, minimizing the error energy function

$$E(\mathtt{A}) = \sum_{i=1}^{N} \Psi \left(-\frac{1}{b_i} \ln \left(\frac{S_i}{S_0} \right) + \mathtt{d}_i^t\mathtt{A}\mathtt{d}_i \right) \tag{1}$$

as a non-linear gradient descent problem. Since $\mathtt{A}$, is estimated in $S^+(6)$, the diffusivity function is guaranteed to be positive definite. We, however, realize that since $\mathtt{A}$ is estimated in $S^+(6)$, it has 21 independent coefficients, while a 4th order diffusion tensor is totally symmetric and has only 15 independent coefficients. This indeterminacy can be overcome by noticing that $\mathbb{G}$ is totally symmetric, therefore

$$D(\mathbf{g}) = tr(\mathbb{A}\mathbb{G}_i) = tr((\mathbb{A}^s + \mathbb{A}^a)\mathbb{G}_i) = tr(\mathbb{A}^s\mathbb{G}_i) \tag{2}$$

where $\mathbb{A}^s$ contains the coefficients of the 4th order diffusion tensor and $\mathbb{A}^a$, the residue, contains the excess parameters. We can, therefore, apply the symmetry constraint of $||\mathbb{A}^a|| = 0$ by projecting $\mathbb{A}$ to its symmetric part $\mathbb{A}^s$.

3 Results

Here we present the details of the various datasets, explain our experiments and their motivations, and finally present the results.

Synthetic Data Experiment. We used a synthetic dataset to compare the robustness of the various methods under varying controlled conditions. The synthetic dataset to simulate fiber-crossings was generated using the multi-tensor model [9]. The synthetic diffusion weighted images S_i were generated from $S_i(b, g_i) = \sum_{k=1}^{n} p_k e^{-bg_i^T \mathbf{D_k} g_i} + \xi$, where b is the b-value, g_i is i-th gradient direction for $i \in \{1, N\}$, $n \in \{0, 1, 2, 3\}$ is the number of fibers and ξ is the Rician noise generated with a complex Gaussian noise with standard deviation of $1/\sigma$, producing an SNR of σ. The diffusion tensor profile used for a single fiber was diag($\mathbf{D_k}$) = [1390,355,355]x10^{-6}mm^2/s and for isotropic voxels was diag($\mathbf{D_k}$) = [700,700,700]x10^{-6}mm^2/s. Crossing voxels were composed of equal volume fractions ($p_k = 1/n$). This synthetic data generation is relatively standard and has the advantage of producing known ground truth ADC and ODF profiles as well as ground truth fiber orientations.

In our experiment to compare robustness, we varied the SNR from $\sigma = 2$ to $\sigma = 50$ to estimate the 4th order diffusion tensor using the different methods. Then we computed the mean and the standard deviation of the squared error between the estimated ADCs and the ground truth ADC. The results are plotted in Fig. 1. We repeated the experiment for $b = 1000s/mm^2$ and for $b = 3000s/mm^2$.

The Riemannian approach compares favourably to the exisiting methods. The TQ method, whose performance may seem surprising, perhaps needs a word of explanation. This was coded by us from [8], using the same guidelines and standards used for the rest of the methods. It seems to us, however, that it is highly sensitive to the optimization algorithm and to the initial conditions used, and we might not have the optimal implementation.

Estimation from Human Brain Data. In the next experiment we used a relatively large human brain dataset of 128 x 128 x 60 voxels for estimation. We used a mask to effectively work on 249352 voxels. This dataset was aquired on a 1.5T scanner at $b = 700s/mm^2$ using 41 encoding directions, with voxel dimensions of 1.875mm x 1.875mm x 2mm[1].

In this experiment we checked the ADC profiles of the estimated tensors on a set of 81 gradient directions distributed evenly on a hemisphere, to examine the compliance of the estimation methods to the positive diffusivity constraint.

[1] The NMR database can be obtained by contacting Cyril Poupon directly by email, cyril.poupon@cea.fr.

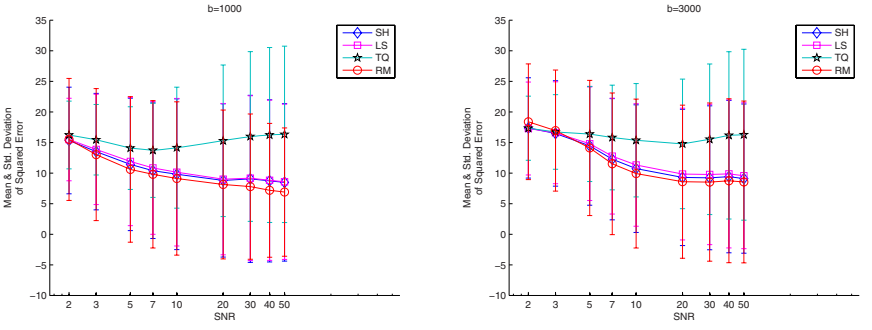

Fig. 1. Comparison of the DTI-4 estimation methods with varying SNR, computed for $b = 1000s/mm^2$ and for $b = 3000s/mm^2$. The SNR varies from $\sigma = 2$ to $\sigma = 50$. The Riemannian approach compares favourably to the exisiting methods.

Table 1. The estimated ADCs from 249352 tensors are checked for positive diffusivity on a set of 81 gradient directions distributed evenly on a hemisphere. The Riemannian and the TQ, are the only methods which guarantee a positive diffusivity profile.

(81 dirs)	LS	SH	TQ	RM
Positive	181757	249263	249352	249352
Negative	67595	89	0	0

Table 2. Time taken to estimate 249352 4th order diffusion tensors from a real dataset. The Riemannian method performs competitively when compared to the LS and SH methods, and still guarantees positive diffusion.

	LS	SH	TQ	RM
Time (sec)	7	28	22526 (6h 15min)	146 (2min 26s)

The results are presented in Table 1. The Riemannian and the TQ, are the only methods which guarantee a positive diffusivity profile.

In this experiment, we also timed the different methods, to compare their running times. It can be expected that as the estimation methods get more complex by trying to accomodate the positivity constraint, they also get computationally expensive. The motivation behind this experiment was to investigate the difference in performances of the simple estimation methods (LS, SH) and the more complex methods (TQ, RM). The results are presented in Table 2. The Riemannian method performs competitively when compared to the LS, and the SH methods, and it still guarantees positive diffusion (Table 1), making it a practical method to apply on large datasets.

Fiber Orientation on Biological Phantom Data. Next we worked on a biological phantom dataset to move beyond the ADC, and to compute the ensemble-average diffusion propagator (EAP) from the 4th order diffusion tensor.

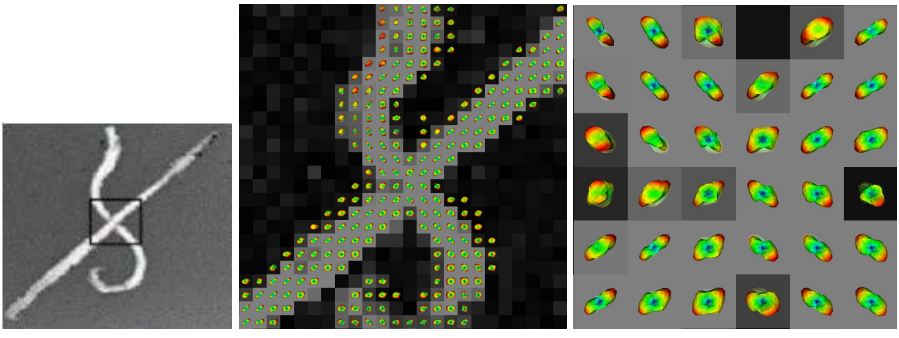

Fig. 2. The ensemble-average diffusion propagator (EAP) in every voxel on a biological phantom data. It is computed from the 4th order diffusion tensor which in turn has been estimated using the Riemannian method. The background is coloured using the GFA, while the glyphs are colour-encoded to indicate directional anisotropy. The image to the right zooms into the crossing section to provide a close up. T1 image to the left.

Since the peaks of the ADC do not necessarily correspond to the orientations of the underlying fiber bundles, it becomes necessary to compute the EAP to infer the correct directions. The EAP, $P(\mathbf{r})$, is given by the Fourier transform $P(\mathbf{r}) = \int E(\mathbf{q}) \exp(-2\pi i \mathbf{q}^T \mathbf{r}) d\mathbf{q}$, where $\mathbf{q}$ is the reciprocal displacement vector, $E(\mathbf{q})$ is the signal value associated with the vector $\mathbf{q}$ divided by the zero gradient signal, and $\mathbf{r}$ is the spin displacement vector. We computed the Fourier Transform numerically to estimate the EAP from the 4th order diffusion tensor.

The phantom contained exactly two fiber bundles, and this provided us with a framework to validate the estimated EAP. The biological phantom was created from two excised rat spinal cords embedded in 2% agar (see [12]). The acquisition was done on a 1.5T scanner using 90 encoding directions, with b = $3000 s/mm^2$, TR= 6.4 s, TE= 110 ms, 2.8 mm isotropic voxels and four signal averages per direction. The SNR of a single DW image in the spinal cord was estimated to be 5 and the corresponding averaged DW image had an SNR value of 10.

Fig 2, provides a qualitative result of the estimated EAP. In the figure each glyph represents an iso-surface of the corresponding EAP. We first estimated the 4th order diffusion tensors using the Riemannian method. Then we numerically computed the Fourier Transform to estimate the EAP. The background is coloured using the Generalised Fractional Anisotropy (GFA)[2], while the glyphs are colour-encoded to indicate directional anisotropy, with red representing high anisotropy and blue representing low values. The image to the right zooms into the crossing section to provide a close up. It can be seen that the EAP provides the correct orientation of the underlying fiber bundles.

Fiber Orientation on Human Brain Data. This dataset was aquired with 60 encoding gradient directions, a b-value of 1000 s/mm^2, twice-refocused spin-echo EPI sequence, TE = 100 ms, GRAPPA/2, 1.72 mm x 1.72 mm x 1.7 mm

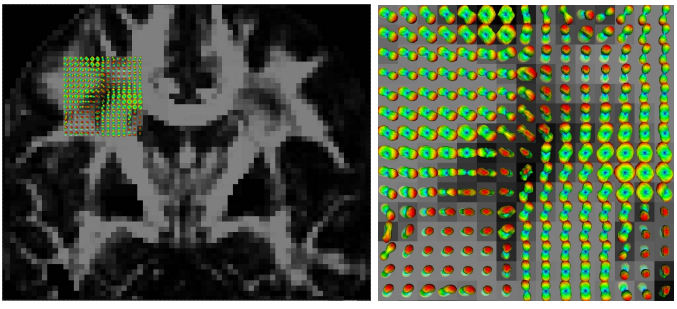

Fig. 3. We used the Riemannian method to estimate the 4th order diffusion tensors in a coronal slice, within a region of interest (ROI). From these we computed the ensemble-average diffusion propagator (EAP). In the ROI we see crossing fibers between the cortico spinal tract, superior longitudinal fibers (traversing the plane) and the corpus callosum (in the plane).

voxel resolution, with three repetitions, and corrected for subject motion. It was acquired on a whole-body 3T Trio scanner.

In this dataset we particularly looked at a Region of Interest (ROI) of a coronal slice, where complex fiber structures are known to exist in the white matter. The ROI contained fiber bundles from the cortico-spinal tract, superior longitudinal fibers (traversing the plane) and the corpus callosum (in the plane). We looked at this ROI to detect these different fiber bundles.

First we used the Riemannian method to estimate the 4th order diffusion tensors in every voxel, and then we computed the Fourier Transform to estimate the EAP.

4 Conclusion

Diffusion MRI is today the cutting edge tool to investigate the human brain anatomy. DTI was the first model proposed, and still remains today of immense value to both the clinician and the neuro-scientist. It has a major shortcoming in regions of fiber crossings, and therefore, other HARDI reconstruction techniques were invented to overcome this limitation. One among these is the HOT model, which has not been extensively researched.

We proposed to take this model further, since sophisticated esimation techniques have been established and well tested for DTI, which guarantee the compliance with the important constraint of positive diffusivity. To that goal we extended the Riemanian framework from DTI to the space of 4th order diffusion tensors. We also compared our Riemannian method to the existing methods on synthetic, phantom and real datasets. We tested all the methods for robustness, speed and also computed the diffusion propagator (EAP) to infer underlying fiber bundle orientations.

In the synthetic dataset tests, the Riemannian method performed well for varying sets of noisy data. This can be attributed to the fact that it inherently satisfies the positive difusivity constraint. This positive diffusivity was confirmed when the method was tested on large real datasets. A feather in the cap was also its computational speed on these large datasets. It performed very competitively when compared to simpler methods like the LS and the SH. Computing the EAP from the Riemannian method also proved to be successful. This was verified qualitatively on a controlled biological phantom, and we also tested the EAP on a real human brain dataset.

In short the performance of the Riemannian method proved to be favourable on all three accounts of robustness and positive diffusivity, computation-time and estimation of the EAP, on synthetic and real datasets. Its fast computational time made it valuable practically. We plan to explore the 4th order tensor model further for fiber-tracking, segmenting and registration in the future.

References

1. Basser, P., Mattiello, J., LeBihan, D.: Estimation of the effective self-diffusion tensor from the NMR spin echo. Journal of Magnetic Resonance B(103), 247–254 (1994)
2. Tuch, D.: Q-ball imaging. Magnetic Resonance in Medicine 52(6), 1358–1372 (2004)
3. Frank, L.: Characterization of anisotropy in high angular resolution diffusion-weighted MRI. Magnetic Resonance in Medicine 47(6), 1083–1099 (2002)
4. Ozarslan, E., Mareci, T.: Generalized diffusion tensor imaging and analytical relationships between diffusion tensor imaging and high angular resolution imaging. Magnetic Resonance in Medicine 50, 955–965 (2003)
5. Liu, C., Bammer, R., Moseley, M.E.: Generalized diffusion tensor imaging (gdti): A method for characterizing and imaging diffusion anisotropy caused by non-gaussian diffusion. Israel Journal of Chemistry 43, 145–154 (2003)
6. Lenglet, C., Rousson, M., Deriche, R., Faugeras, O.: Statistics on the manifold of multivariate normal distributions: Theory and application to diffusion tensor MRI processing. Journal of Mathematical Imaging and Vision 25(3), 423–444 (2006)
7. Arsigny, V., Fillard, P., Pennec, X., Ayache, N.: Log-Euclidean metrics for fast and simple calculus on diffusion tensors. Magnetic Resonance in Medicine 56(2), 411–421 (2006)
8. Barmpoutis, A., Jian, B., Vemuri, B.C.: Symmetric positive 4th order tensors & their estimation from diffusion weighted MRI. In: Karssemeijer, N., Lelieveldt, B. (eds.) IPMI 2007. LNCS, vol. 4584, pp. 308–319. Springer, Heidelberg (2007)
9. Descoteaux, M., Angelino, E., Fitzgibbons, S., Deriche, R.: Apparent diffusion coefficients from high angular resolution diffusion imaging: Estimation and applications. Magnetic Resonance in Medicine 56, 395–410 (2006)
10. Moakher, M.: The algebra and geometry of fourth-order tensors with application to diffusion MRI. In: Weickert, J., Hagen, H. (eds.) Perspectives Workshop: Visualization and Image Processing of Tensor Fields, vol. 04172 (2006)
11. Basser, P.J., Pajevic, S.: Spectral decomposition of a 4th-order covariance tensor: Applications to diffusion tensor MRI. Signal Processing 87, 220–236 (2007)
12. Savadjiev, P., Campbell, J.S.W., Pike, B.G., Siddiqi, K.: 3D curve inference for diffusion MRI regularization and fibre tractography. Medical Image Analysis 10, 799–813 (2006)